Absolute electron temperature estimates from the intensity of a single spectral line in radiation dominated plasmas

C.A. Michael* and J. Howard
PRL, RSPhysSE, Australian National University, Canberra A.C.T. 0200 Australia
(Dated: April 11, 2004)

We describe a novel technique to absolutely estimate the electron temperature in radiation dominated plasmas from the temporal decay during the plasma afterglow of the intensity of a single spectral line. The model and underlying assumptions are described. We apply the model to data in both RF heated argon discharges and ECH heated He/H discharges in the H-1 Heliac. The results agree well with probe measurements.

PACS numbers:

I. INTERPRETATION OF SPECTRAL LINE INTENSITY

Spectral line intensities convey information about the electron density and temperature, as well as the emitting species density. Generally, collisional-radiative models are used to relate these quantities to the emission spectrum. Low-temperature plasmas, which do not have a significant population of meta-stable states can be regraded as being in coronal equilibrium. For this model, the power radiated per unit volume into a spectral line of the primary ionic species (with upper state is labeled by j and lower state is labeled by i), P_{ij} can be related to the electron density n_e and electron temperature T_e through [1]:

$$P_{ij} = k_{ij} n_e^2 \xi_{ex}(T_e, \chi_j) \tag{1}$$

where we have set the ion density equal to n_e through quasi-neutrality, since in radiation dominated low temperature plasmas, the abundance of species with $Z > 1$ is negligible. This is verified in H-1 by the absence of any corresponding spectral lines. The constant k_{ij} is dependent only on atomic rate coefficients for the particular transition, and the excitation rate coefficient $\xi_{ex}(T_e, \chi_j)$ is dependent on the excitation potential χ_j through:

$$\xi_{ex}(T_e, \chi_j) = T_e^{-1/2} \exp(-e\chi_j / k_B T_e) \tag{2}$$

The detected spectral line intensity is therefore given by $I_{ij} = c(\lambda) P_{ij}$ where $c(\lambda)$ a wavelength-dependent calibration constant, dependent only on properties of the detector and light collection system.

The electron temperature can be obtained from spectral line ratios of the same species, based on relative calibration $c(\lambda_1)/c(\lambda_2)$. In low temperature argon, using the coronal model, this is impractical, however, since the range of values of χ_j accessed by different spectral lines is too small to deliver reliable measurements. However, this has been done in helium using full collisional-radiative models [2].

*Electronic address: Clive.Michael@anu.edu.au

Alternatively, T_e may be determined given independent measurements of n_e, as well as the absolute calibration constant $c(\lambda)$. Absolute calibration can be difficult, however, since it requires an accurate knowledge of the etendue of the source region, transmission efficiency of the optical system and absolute detector response. In practice, it is simpler to infer the absolute calibration constant $c(\lambda)k_{ij}$ from a single independent measurement of T_e (for example, from a Langmuir probe). Another problem with this technique is that the strong non-linearity of $\xi_{ex}(T_e)$ can result in very large amplification of errors.

When the electron power balance is dominated by radiation, the characteristic shape of the decay curve of $I(t)$ depends on the electron temperature at the time of the heating power switch off. This is the basis of the model for obtaining T_e, described in section II. In section III, we discuss the fitting procedures and the apply this model to intensity profile data, measured using a coherence imaging camera [3] on the H-1 Heliac [4]. The inferred temperature profiles are compared with probe measurements.

II. MODEL DESCRIPTION

The model is based on the electron power balance during the plasma afterglow, following the termination of the heating pulse. In H-1, we find that the density decays slowly during this phase, on a time-scale of the order of 3-5ms, while the intensity decays in around 100μs. However, in the steady state, the particle confinement time can be estimated from particle balance to be $\sim 100\mu$s. Since this is significantly different from the density decay time, there must be a rapid re-arrangement of the plasma potential to improve particle confinement. Because the density decays much more slowly than the intensity, convective energy losses are negligible in the afterglow. During the discharge, however, convective energy losses may be significant.

The remaining (non-convective) electron energy loss mechanisms are radiation, ionization of neutrals and diffusive thermal transport. It is well known that in low temperature discharges, radiation can account for a substantial fraction the total electron input power. In

this model, we consider only ionization (P_{iz}), radiation from neutrals ($P^{\rm I}_{rad}$) and from ions ($P^{\rm II}_{rad}$): $P_{tot}(T_e) = P^{\rm II}_{rad} + P^{\rm I}_{rad} + P_{iz}$, where each term is related to T_e, n_e, and n_n through:

$$P^{\rm II}_{rad}(T_e) = \sum k_{ij} n_e^2 \xi_{ex}(T_e, \chi_j) \quad (3)$$

$$P^{\rm I}_{rad}(T_e) = \sum k_{ij} n_e n_n \xi_{ex}(T_e, \chi_j) \quad (4)$$

$$P_{iz}(T_e) = k_{iz} n_e n_n \xi_{iz}(T_e, \chi_{iz}) \quad (5)$$

Where ξ_{iz} is the ionization rate coefficient. For Ar II, the brightest spectral lines have their excitation potentials χ_j clustered around $\chi_{\rm II} = 19$eV, and for Ar I, χ_j are clustered around $\chi_{\rm I} = 15$eV [5]. Furthermore, for $T_e \lesssim 5$eV, $\xi_{iz}(T_e, \chi_{iz}) \approx$ const $\times\, \xi_{ex}(T_e, \chi_{\rm II})$ (since $\chi_{iz} = 15.75$eV, and the classical exchange impact approximation for ξ_{iz} is close to that of ξ_{ex} [1]). This feature is not unique to argon - the excitation energies spectral lines of most species are clustered around certain values. Therefore, we take the T_e dependence of P_{tot} as being proportional (through constant b) to the excitation rate coefficient of a single ionic spectral line (which we now denote by subscript λ_1):

$$P_{tot}(T_e) = b n_e (n_e + \alpha n_n) \xi_{ex}(T_e, \chi_{\rm II}) \quad (6)$$

where $\alpha = (P^I_{rad} + P_{iz})/P_{tot}$.

During the afterglow, the electron stored energy decays as $dW_e/dt = P_{tot}$. Expressing $W_e = n_e T_e$, and given that the density remains constant on the intensity decay time-scale, we can write the following equations which can be solved for $T_e(t)$ and $I_{\lambda_1}(t)$:

$$\frac{dT_e(t)}{dt} = b' \xi\big(T_e(t), \chi_{\rm II}\big) \quad (7)$$

$$I_{\lambda_1}(t) = c' \xi\big(T_e(t), \chi_{\rm II}\big) \quad (8)$$

$$T_e(t_0) = T_{e0} \quad (9)$$

where $b' = b(n_e + \alpha n_n)$, $c' = c(\lambda_1) k_{\lambda_1} n_e^2$, and the RF power is switched off at $t = t_0$. The coefficient b' determines the time-scale of the temperature decay, while the coefficient c', determines the initial intensity. Consequently, discharges with higher density decay on a slower time-scale and from a larger initial intensity. An uncalibrated value for the electron density can be determined from $\sqrt{c'}$ (which effectively uses the inferred value of T_e to convert a relatively calibrated intensity profile into a relatively calibrated electron density profile).

The function $T_e(t)$, can be determined numerically from Eq. (7) and (9), for a given value of b' and T_{e0}. Based on this, the measured intensity $I_{\lambda_1}(t)$ can be computed, given c'. Therefore, the curve $I_{\lambda_1}(t)$ can be parameterized by the three quantities T_{e0}, c' and b'. By fitting the measured curve $I_{\lambda_1}(t)$ to the model described by Eqs. (7-9), these three parameters can be extracted. The χ^2 residual gives an indication of validity of the approximation in Eq. (6).

To illustrate the measurement principle, the calculated decay of the intensity and electron temperature as a function of time are shown in Fig. (1) for three initial temperatures. The characteristic shape of the light intensity decay curve depends on the initial temperature. For high T_{e0}, the rate of decrease of the intensity increases up to a point where $T_e = 2\chi/3$, then starts to decrease again, until $T_e \sim 0.1\chi \sim 2$eV, where only electrons in the tail of the distribution function have energies $E > \chi$, sufficient for radiative decay.

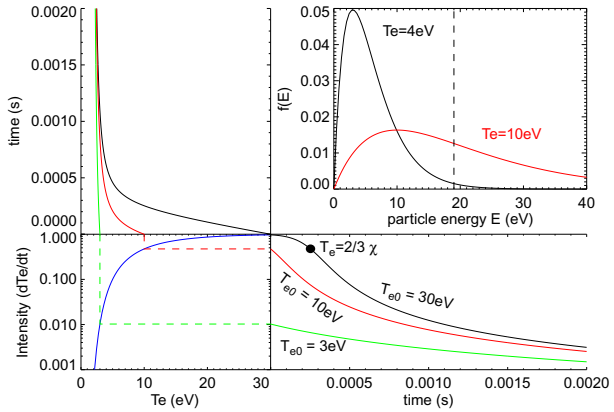

FIG. 1: Decay of electron temperature and light intensity with time, together with their coupling on the I vs T_e curve, and the distribution functions at $T_e = 10$eV and $T_e = 4$eV, showing the difference in the available populations which have energy $E > \chi$ necessary for excitation and radiative decay.

During the decay, the electron collision frequency is typically $\gtrsim 2 \times 10^6 \mathrm{s}^{-1}$, so that the decay time-scales of $\sim 50 - 100\mu$s, at least 100 collisions can occur, maintaining the distribution function Maxwellian.

III. ANALYSIS AND RESULTS

We have used the Levenberg-Macquardt (LM) method [6] is for fitting the N discrete intensity measurements (t_i, I_i) to the model $I_{\lambda_1}(t)$ over the time interval $[t_0, t_0 + \Delta t]$, which minimizes the weighted χ^2 residual, defined as:

$$\chi^2 = \sum_{i=1}^{N} [w_i (I_i - I_{\lambda_1}(t_i)]^2 \quad (10)$$

It is necessary to make an appropriate choice for the weights w_i, the duration of the fit Δt as well as the time t_0 of the termination of the heating pulse. Though the latter can be obtained directly by monitoring the heating power, uncertainties of the order of $\sim 10\mu$s can have a significant effect on T_{e0}, since the initial decay conveys most of the information. We consider setting $w_i = I_i^{-p}$, with $p = 0, \frac{1}{2}, 1$. By setting $p = 1$, each data point is contributes equally to the χ^2 residual, so that the choice of Δt affects the inferred value of T_{e0}. On the other hand, for $p = 0$, points of lower intensity convey very little contribution to χ^2 so that the choice of Δt does not significantly affect the fit. It is strictly

correct to set $p = 1/2$, since light has a Poissonian noise distribution. However, we choose to set $p = 0$ since the model is less valid when the light intensity (and electron temperature) decrease to a point where radiation is no longer the dominant energy loss mechanism. We have defined the standard errors in T_{e0}, b' and c' according to the standard definition in the absence of measurement errors [6], such that $\Delta\chi^2 = \chi^2/(N-M)$ (where $M = 3$ is the number of fitted parameters).

Spectral line intensities on the H-1 Heliac were measured with a coherence imaging camera [3], a fixed delay Fourier transform spectrometer delivering only the spectral line intensity, central frequency and width. The instrument images a poloidal cross-section of the plasma, and after signal processing, the data is sampled at 50kHz, sufficient to track the intensity decay. We present data from three discharges: L (non-fluctuating) and H (fluctuating) modes of RF-heated argon plasmas (for which we use the Ar II line $\lambda = 488$nm, with $\chi_{II} = 19$eV) and an ECRH He/H discharge for which we monitor He II at $\lambda = 468$nm (with $\chi_{II} = 54$eV). The decay of the local (Abel inverted) intensity, together with the fitted intensity decay at various radial positions is plotted in Fig. (2) for H-mode RF heated argon and ECRH He discharges. We find that the conformity of the data to the fit is best in the initial decay phase, indicating that as the temperature decreases, the model breaks down.

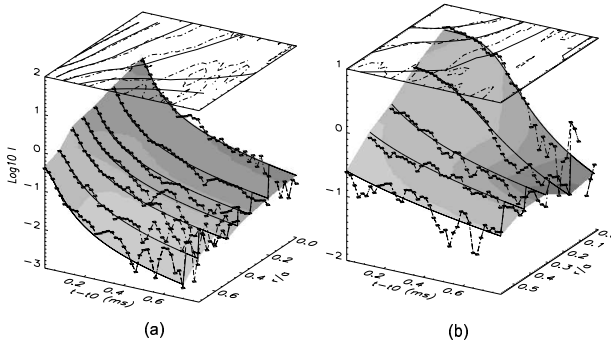

FIG. 2: Logarithm of the intensity decay for different radial positions, together with model fits, in (a) H-mode RF heated argon discharge ($B = 0.09$T, $P_{\rm fill} = 36\mu$Torr, $P_{rf} = 60$kW), and (b) ECRH He/H discharge (???)

Radial profiles of the inferred electron temperature and density (from $\sqrt{c'}$), in both L and H modes of RF heated argon discharges are plotted in Fig. (3). The T_e profiles are compared with probe measurements [7], while the n_e profiles are compared with line-integrated electron density measurements using a 2mm interferometer. (The absolute value of the densities given are obtained from a common calibration constant, equal to the mean of the calibration constants in each case.) The comparison of the relative scaling of the inferred line integrated density between L and H modes with the interferometer signals provides another test of the accuracy of the inferred values of T_e. The probes give excellent agreement with the inferred temperature everywhere in H-mode, while agreeing better in the centre for L-mode. The error bars are larger for L mode due to the presence of density fluctuations and faster decay rates (on account of lower density in spite of higher temperatures). The presence of fluctuations in L mode may also produce erroneous values of T_{e0} since this violates the model assumption of constant density.

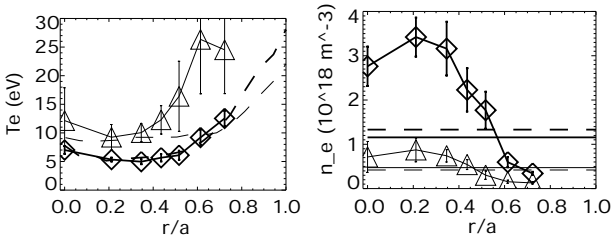

FIG. 3: Profiles of inferred electron temperature (a) and density (b) (solid line), in L-mode (thin line) and H-mode (thick line). In (a), the equivalent probe measurements are indicated by the dashed line. In (b), the solid horizontal line indicates the computed line average, while the the dashed line indicates the 2mm interferometer measurement.

The inferred T_e profile for the ECRH discharge is plotted in Fig. (4), showing central peaking. This can feature is clearly visible in the raw data, since the central regions show light persisting much longer than the edge channels. The large variation in T_e rendered the error bars in the n_e profiles too large to be of use. Though no independent measurement could be made, the centrally peaked profile is characteristic of ECRH discharges.

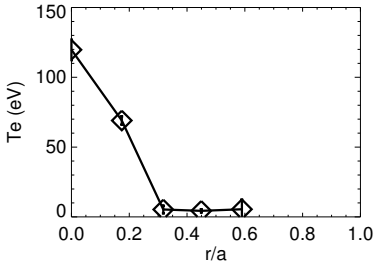

FIG. 4: Electron temperature profile for the ECRH discharge

While the assumptions underlying the power balance in Eq. (6) are strong, this technique is useful for obtain simple estimates of T_e in the absence of any other measurements, in radiation dominated plasmas, (generally where $T_e \lesssim 2\chi_{II}$).

[1] I. H. Hutchinson, *Principles of plasma diagnostics* (Cambridge University Press, Cambridge [Cambridgeshire] ; New York, 1987).
[2] A. R. Field, P. G. Carolan, N. J. Conway, and M. G. O'Mullane, AIP. Review of Scientific Instruments **70**, 355 (1999).
[3] C. A. Michael, J. Howard, and B. D. Blackwell, Review of Scientific Instruments **72**, 1034 (2001).
[4] S. M. Hamberger, B. D. Blackwell, L. E. Sharp, and D. B. Shenton, Fusion Technology **17**, 123 (1990).
[5] *National institute of standards atomic spectroscopy database.*
[6] W. H. Press, *Numerical recipes in C: the art of scientific computing* (Cambridge University Press., Cambridge, 1992).
[7] M. G. Shats, D. L. Rudakov, R. W. Boswell, and G. G. Borg, Physics of Plasmas **4**, 3629 (1997).